Performance Investigation of Flexible UWB Antenna near Human Body for Wearable Appliances

Mamta D. Sharma[1, *], Ajay Yadav[2], Sarthak Singhal[1, *], and Ritu Sharma[1]

Abstract—A very economical and compact size wearable antenna operating over Ultra-Wide Band (UWB) spectrum is investigated in the proposed work. The antenna is modelled on a thin FR-4 (0.2 mm) material that makes it flexible and well-suited for wearable appliances. The radiating patch structure is the combination of one square and two elliptical patches rotated at 45° and fed with a Coplanar Waveguide (CPW) to achieve a wide impedance bandwidth. The complete radiating structure looks like a flower shape, and it has a partial ground to support the radiation from the antenna over the complete UWB. The flexibility of the proposed structure is investigated by bending it along xz and yz planes using cylindrical shape foam. The peak Specific Absorption Rate (SAR) is demonstrated for 1 g and 10 g of tissues at different chosen frequencies like 3.7, 8.4, and 11.2 GHz using a three-layer phantom model. The presented antenna performance analysis and compact size confirm that it is a good candidate for wearable applications.

1. INTRODUCTION

In the current scenario of the COVID-19 pandemic, healthcare practitioners are fighting to avoid spreading the infection by increasing contactless medical measures. To evade contact with the patients, to assure safety and to provide remote monitoring, wireless communication devices and systems are recommended by medical experts that can help to take follow-up vital signs of the patients [1]. The current demand from the medical industry has increased the attention of researchers toward the development of wireless medical devices and sensors. These wireless medical devices and sensors are used to share the vital signs with the doctor and get feedback from a doctor through antennas. These antennas must have to keep critical characteristics like flexibility, compact size, light-weight, easy production, easy integration with other electronic modules, minimum back radiations, satisfactory gain, and broad impedance bandwidth [2]. Designing a wideband antenna that can operate over short-range communications for a *Wireless Body Area Network* (WBAN) is a very challenging task. These antennae must operate close to the human body's suitable medium. However, these antennae placed over the human body suffer from the problems like detuning of resonance frequencies. Antenna performance parameters are also altered when it is bent or rolled.

After the avowal of the UWB spectrum in 2002 for commercial applications by the *Federal Communications Commission* (FCC) [3], the UWB antenna has gained more attention from investigators due to its significant merits. It has immunity to electromagnetic interference with other medical signals, robust to fading, possesses a high data rate, and needs less power to operate. So, it cannot affect the human tissues. According to a recently reported studies on the wearable antenna,

monopole structures are extensively used for many applications, such as wireless communication, body area network (BAN), biomedicine, microwave imaging, and cancer screening [4–6].

To enhance the bandwidth of the antenna, numerous modifications in geometry have been reported, such as the use of Ashoka chakra shaped as radiating part and triangular truncated corners in the ground plane [7], perforated in the ground radiator with the corner cut top rectangular patch [8], fractal structures [9], and slots of different shapes [10], T-shaped [11], L-shaped [12], crescent shape [13], staircase-shaped slits [14], and flower-shaped patch [15]. These methods are useful to the design of a wideband antenna for wearable applications. Also, various flexible UWB antennas have been designed on polyimide, polyamide, Teslin, PDMS, and textile with different shapes for wearable applications [16–19, 20]. For wearable applications, UWB antennas have been investigated to validate their performance near human tissues and their impacts on body tissues in [21] and [22].

The presented work has a flower-shaped UWB antenna that is flexible in nature and compact in size. It is fabricated on a thin FR-4 substrate which makes it very economical in comparison to other conventional wearable antennas. It can be easily fabricated using the chemical etching technique which makes it economical whereas it is also compatible with other fabrication techniques.

To validate the wearable compatibility of the presented antenna, the S_{11} response for distinct bend situations, radiation characteristics, gain, and SAR are demonstrated. The proposed antenna is robust and flexible which makes it favorable for wearable applications. It has $50°$ of freedom for bending in xz and yz planes with a very consistent gain of approximately $4\,\text{dB}$ and wide bandwidth whereas the compact size is its added advantage. The manuscript is organized as follows. Section 2 describes the antenna design and simulation. Section 3 presents the simulated and measured results of the antenna when it is bent on xz and yz planes. Sections 4 and 5 present the antenna performances for time domain and in free space along with proximity of the human phantom respectively. Last, Section 6 includes the key findings and possible improvements in future work as the conclusion.

2. ANTENNA DESIGN AND SIMULATION

2.1. Antenna Design and Evolution

The design and evolution of the presented antenna are performed with the commercially available electromagnetic simulator CST Microwave Studio. The primary radiating structure (Antenna-I) is a square-shaped monopole rotated at $45°$ and fed with a coplanar waveguide (CPW) as shown in Figure 1(a). Further, two orthogonal elliptical radiating patches rotated at $45°$ are added with the primary antenna to increase the bandwidth as exhibited in Figure 1(b). The Antenna-II design is sufficient to achieve the UWB spectrum; however, to increase the upper end of the UWB spectrum and provide a better impedance matching, the side edges of the ground radiator are truncated at $6°$ as presented in Figure 1(c).
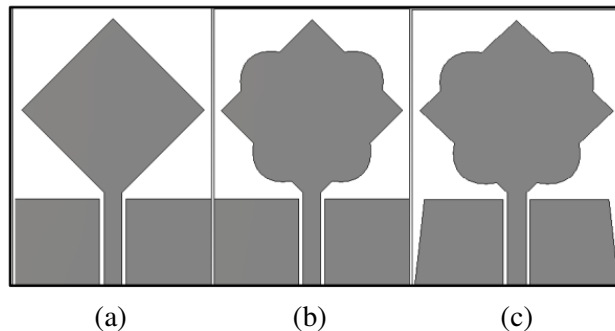
Figure 1. Design and evolution of the suggested antenna. (a) Antenna-I. (b) Antenna-II. (c) Proposed antenna.

The suggested antenna is designed on a lightweight and economical FR-4 dielectric with $0.2\,\text{mm}$ breadth. The substrate permittivity is 4.4 and the loss coefficient ($\tan\delta$) 0.02. Simulated snapshots with dimension variables are presented in Figure 2.
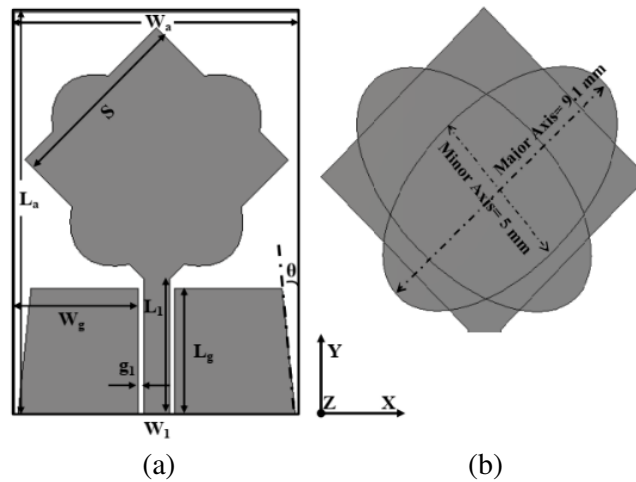
Figure 2. (a) Configuration of the simulated UWB antenna. (b) Radiator structure. ($W_a = 22$, $L_a = 31$, $W_g = 9.5$, $W_1 = 2$, $L_g = 9.65$, $L_1 = 10.4$, $S = 14.4$, $g_1 = 0.5$ and $\theta = 6°$). (Apart from angle all magnitudes are in mm).
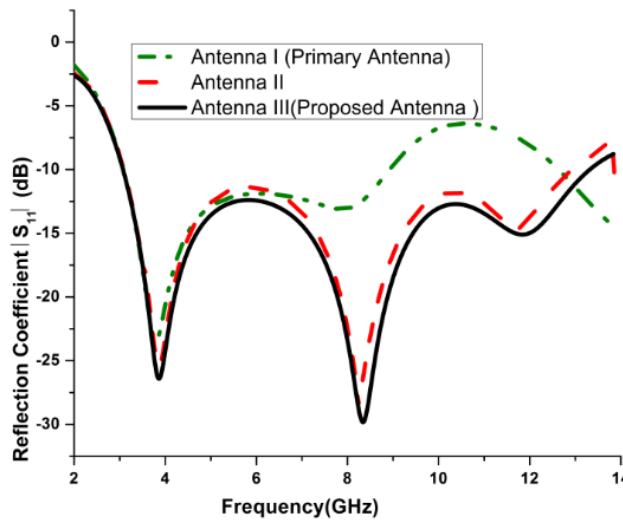
Figure 3. Simulated magnitude of S_{11} (dB) with different configuration.

The reflection coefficient (S_{11}) for stepwise evolution is shown in Figure 3. The primary configuration is (Antenna-I) a $45°$ rotated square radiator with a $50\,\Omega$ CPW feed-line of the width of $2\,\text{mm}$ and a rectangular partial ground radiator that operates in the frequency band from 3.1 to 8.9 GHz. This configuration fails to achieve the entire UWB spectrum and has poor impedance matching. So, a modified shaped patch structure (antenna II) is adopted to enhance the perimeter of the radiating patch, which improves the impedance matching at higher-order resonant frequencies, and it accommodates the complete UWB spectrum. Furthermore, the final proposed configuration is the same as that used in the previous (antenna II) configuration, but the ground plane is truncated by $6°$ at the side edges to improve the impedance matching as seen in Figure 3. This configuration resonates from 3.08 to 13.3 GHz frequency band.

The presented antenna is flexible in nature, and its xz and yz plane bending is presented in Figure 4. The bending effects on reflection coefficient and radiation patterns are discussed in the next sections. The bending properties of the suggested antenna up to $50°$ are discussed in terms of simulated and measured reflection coefficient and radiation characteristics.
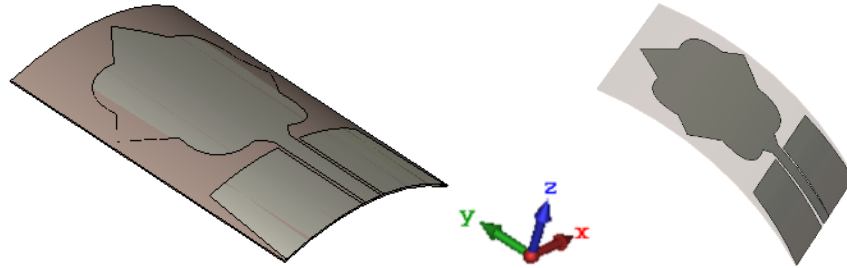
Figure 4. Bending (xz and yz plane) configuration of suggested antenna.

2.2. Measured and Simulated S_{11} (dB) of Proposed Antenna

The antenna prototype was fabricated with the chemical etching method, and a double-sided copper layered FR-4 PCB was used for the desired design pattern. The design pattern film was developed and printed over the FR-4 substrate and followed the chemical etching process. During the fabrication process, desired tolerance limit to get better results was adopted. A prototype of the suggested antenna is presented in Figure 5(a). The fabricated prototype is also checked for its flexibility, and it is observed that the antenna has desired limit of flexibility for wearable applications. The modeled antenna in bent mode is exhibited in Figure 5(b). After the fabrication of the antenna prototype, it is very essential to check whether it has compatibility with the simulated, measured reflection coefficients or not. The antenna's fabricated prototype was measured with a vector network analyzer for its reflection coefficient and compared with the computer-simulated result; it is detected that the results are very close to each other. The reflection coefficient results of the demonstrated antenna are presented in Figure 6.

As perceived in Figure 6, the simulated antenna has a -10 dB of S_{11} for the frequency band between 3.08 and 13.30 GHz whereas the measured bandwidth is between 3.16 and 13.36 GHz. So, it is confirmed that the antenna has satisfactory results of S_{11} for the entire UWB spectrum and has a slight shift in

Figure 5. Photographs of the fabricated. (a) Flat. (b) Bent in yz plane.
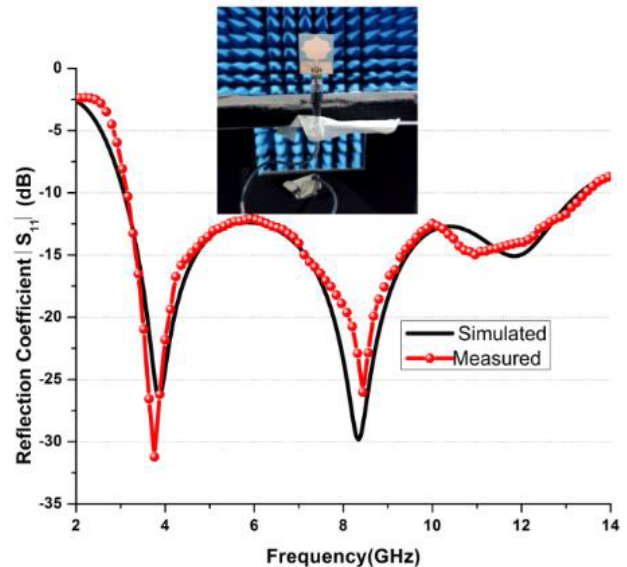
Figure 6. Simulated and measured S_{11} (dB) UWB antenna of the suggested antennas using FR-4.

the lower cut-off frequencies. This variation is found in measured outcomes due to fabrication tolerance and cable losses in the measurement setup.

3. STUDY OF BENDING EFFECTS ON ANTENNA PARAMETERS

3.1. Antenna Scattering Characteristics

The flexible antennas are designed to be positioned on the user's body parts like chest, arm, shoulder, wrist, and joints which get mechanically deformed or alter the antenna's performance with body part movements. To evaluate the bending effects, the proposed UWB antenna is bent over cylindrical foam along the x-axis and y-axis, respectively, at distinct angles such as $10°$, $30°$, and $50°$, which is approximately the size of an adult human and child's forearm [23] and presented in Figure 7. The relationship between the radius of cylindrical foam and bending angles is computed by using the arc length equation [24].
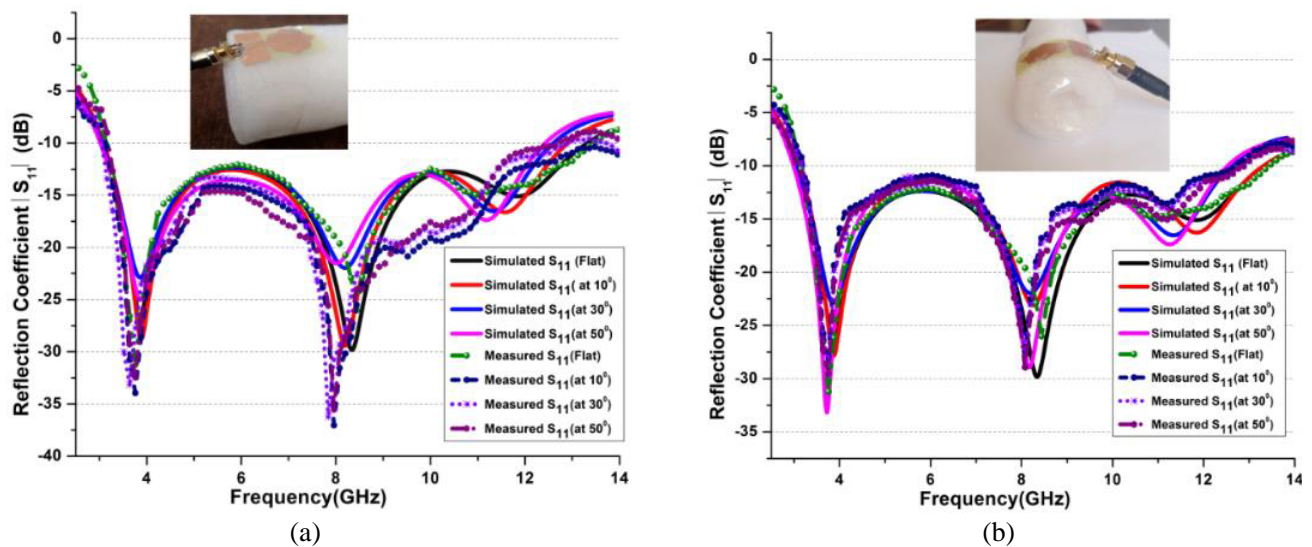
Figure 7. S_{11} (dB) of antenna for bending in (a) xz-plane. (b) yz-plane at different angles (simulated and measured).

Figures 7(a) & (b) show the compared graphs between simulated and measured S_{11} (dB) of the suggested UWB antenna in flat and bending conditions in the xz and yz planes, respectively. It is observed that the operating frequency band of the suggested antenna is affected by bending but still works in the wide UWB. It is clear from the results plotted in Figures 7(a) & (b) that a slight shifting is observed at higher resonance frequencies with an increase in bent angle, whereas at lower frequencies a small variation is observed. So, it is validated that if the structure is placed on an adult human or child's arm, legs, and shoulder, it will properly radiate EM signals in the entire UWB without any significant variations. The measured results of xz and yz plane bending in the antenna are very close to the simulated results. It is shown that the antenna has the potential to deliver very constant and reliable performance in bending conditions. However, it can also be used as a conformal antenna for low-power drive applications.

3.2. Bending Effects on Antenna Far Field Characteristics

The far-field characteristics of the proposed antenna are measured in an anechoic chamber, the cable losses were compensated through the calibration process. The radiation characteristics namely gain and group delay were measured in an anechoic chamber. The simulated and measured radiation patterns are plotted at 3.7 GHz, 8.4 GHz, and 11.2 GHz and are presented in Figures 8 & 9 for xz and yz-plane
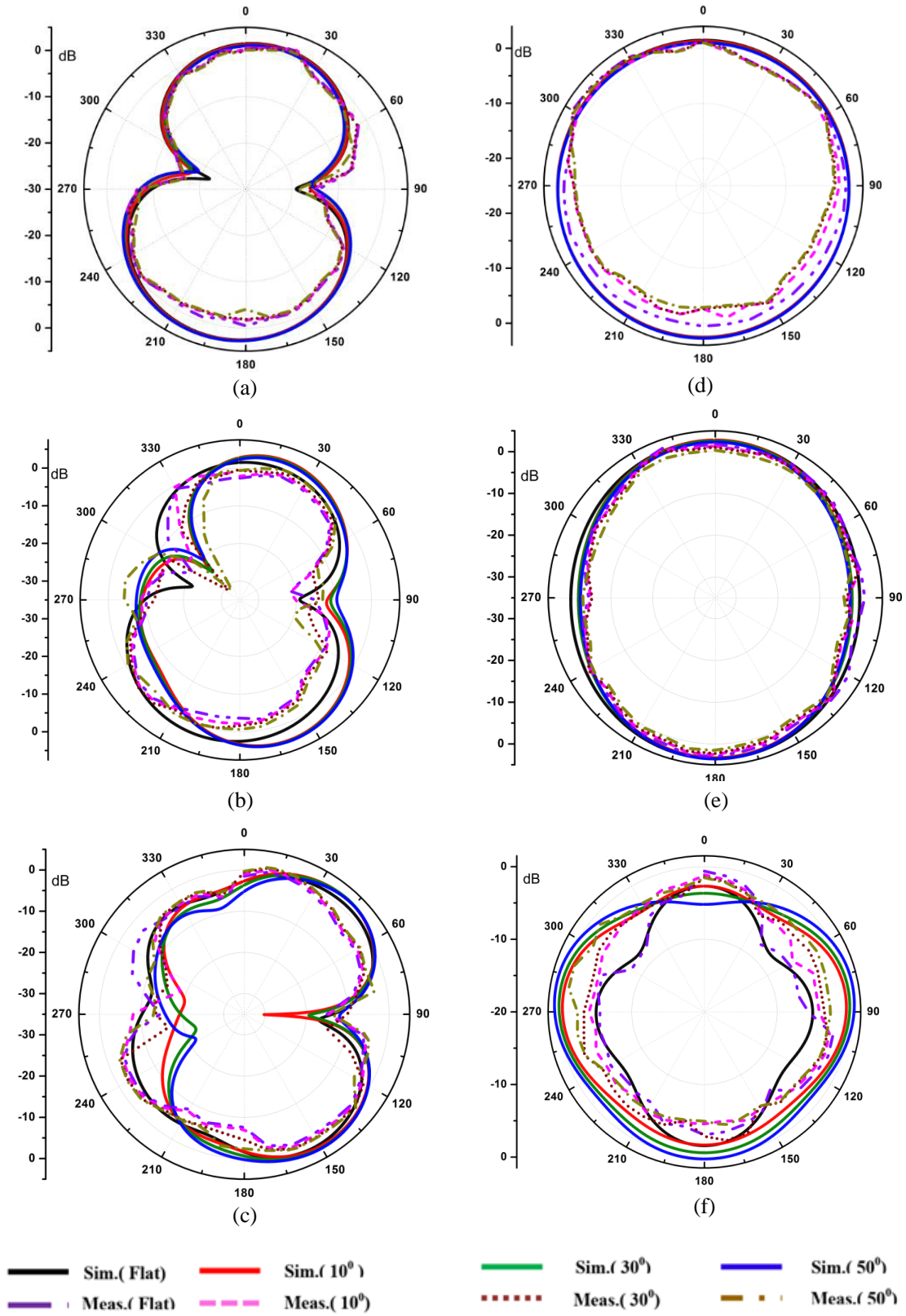
Figure 8. Simulated and measured radiation pattern for different bending angles in xz-plane. (a) 3.7 GHz, (b) 8.4 GHz, (c) 11.2 GHz, (d) 3.7 GHz, (e) 8.4 GHz, (f) 11.2 GHz.
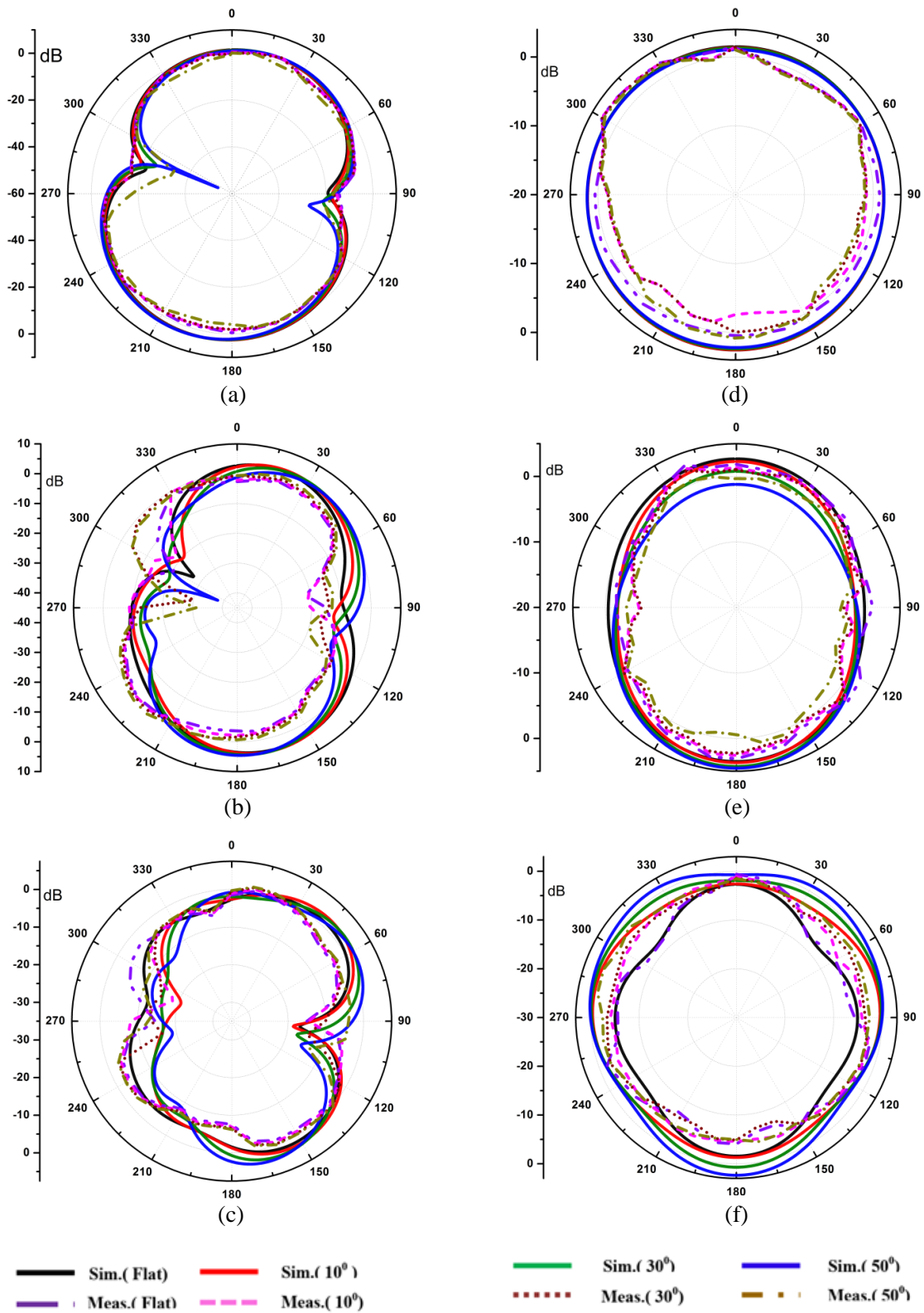
Figure 9. Simulated and measured radiation pattern for different bending angles in yz-plane. (a) 3.7 GHz, (b) 8.4 GHz, (c) 11.2 GHz, (d) 3.7 GHz, (e) 8.4 GHz, (f) 11.2 GHz.

bending, respectively. The proposed UWB antenna has an omnidirectional pattern in the yz-plane and bidirectional radiation pattern in the xz-plane at the lower frequencies, but at higher frequencies, it is distorted due to the entry of higher-order modes. Figures 8(a) to (f) & Figures 9(a) to (f) depict radiation patterns for flat and bending states. A visible variation in the xz-plane pattern is detected at a high frequency in bending conditions; however, it maintains a dipole-like pattern in E-plane, whereas in H-plane the antenna maintains omnidirectional pattern during the bending conditions up to $50°$.

Figure 10 exhibits the gain plots of the designed UWB antenna, and it is noticed that the obtained maximum peak realized gain is around $4\,$dB. Table 1 shows the working bands and gains, respectively, in flat and different bending states. It is indicated that the antenna has satisfactory and nearly constant gain besides the coverage of wideband in all circumstances.
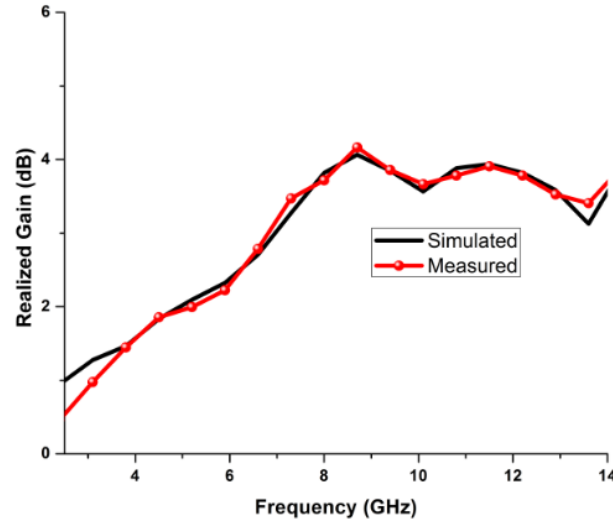
Figure 10. Peak realized gain.

Table 1. Antenna performance at different bending positions.

Position	Effective Frequency Band (GHz)	Peak Gain (dB) at		
		3.8	8.7	11.2 GHz
Flat	3.08–13.30	1.46	4.06	3.93
Bent in XZ-plane (at 10°)	3.07 to 12.90	1.5	4.07	3.85
Bent in XZ-plane (at 30°)	3.05 to 12.60	1.36	4.26	3.70
Bent in XZ-plane (at 50°)	3.03 to 12.42	1.5	4.43	3.66
Bent in YZ-plane (at 10°)	3.1 to 13.30	1.43	4.03	3.76
Bent in YZ-plane (at 30°)	3.05 to 12.59	1.62	4.16	3.66
Bent in YZ-plane (at 50°)	3.0 to 12.52	1.68	4.11	3.45

4. TIME-DOMAIN ANALYSIS

The time-domain characteristics are studied to validate the performance of the proposed antenna in pulsed communication, microwave imaging, and body-worn antennas. These analyses show that group delay, phase response, and system fidelity factor are parameters that confirm the antenna performance in the time domain. Above mentioned parameters are examined by placing two similar antennas in two different orientations at a distance of 15 cm, as seen in Figure 11. In this system, one antenna is transmitting UWB impulse signals while the other is receiving these signals.

(a)

(b)
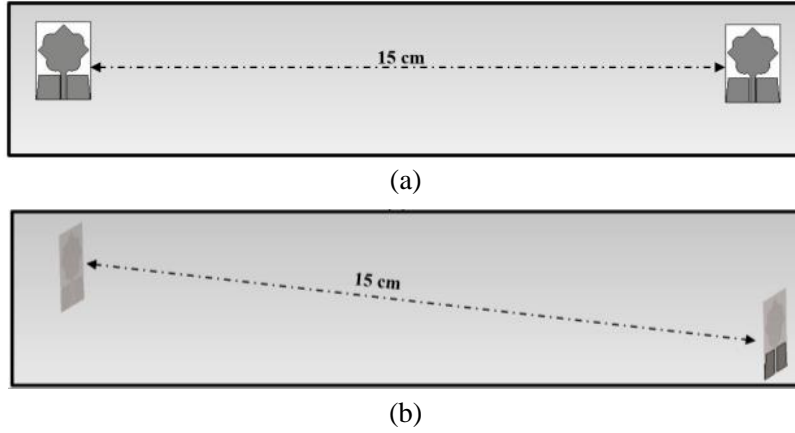
Figure 11. Orientations of the proposed antenna for time domain analysis. (a) Face to face. (b) Side by side arrangement.

The **fidelity factor (FF)** quantifies the degree of resemblance between the transmitted pulse and received pulse. The normalized transmitted $(\hat{T}_S)$/received $(\hat{R}_s)$ signals are given in Equations (1) and (2) [21]:

$$\hat{T}_S = \frac{T_S(t)}{\left[\int_{-\infty}^{\infty} |T_S(t)|^2 \, \mathrm{d}t\right]^{1/2}} \tag{1}$$

$$\hat{R}_s = \frac{R_S(t)}{\left[\int_{-\infty}^{\infty} |R_S(t)|^2 \, \mathrm{d}t\right]^{1/2}} \tag{2}$$

The fidelity factor is calculated by Equation (3)

$$FF = \max_{T} \int_{-\infty}^{\infty} \hat{T}_s \hat{R}_s \, (t + \tau) \, \mathrm{d}t \tag{3}$$

where τ is the delayed time between the transmitted pulse at port 1 and the received pulse at port 2, and $T_s(t)$, $R_S(t)$ are the transmitted and received signals. As FF is calculated result of normalization, the value of FF ranges in the middle of 0 and 1. High values of FF confirm low distortion in the received signal. From Figure 12, it is noted that the FF between transmitted and received signals is around 93.5% and 80% in face-to-face and side-by-side arrangements, respectively.

Group delay is the measure of time delay that occurs between the transmitted signal and received signal. The designed antenna group delay (τ) is presented in Figure 13, and it is noticed that the minimum value of τ is within 1 ns. This response indicates that the proposed antenna has a linear phase response.

The **isolation Coefficient** (S_{21}) is another important parameter that measures the correlation between the transmitted signal and received signal. From Figures 14(a) & (b) it is observed that
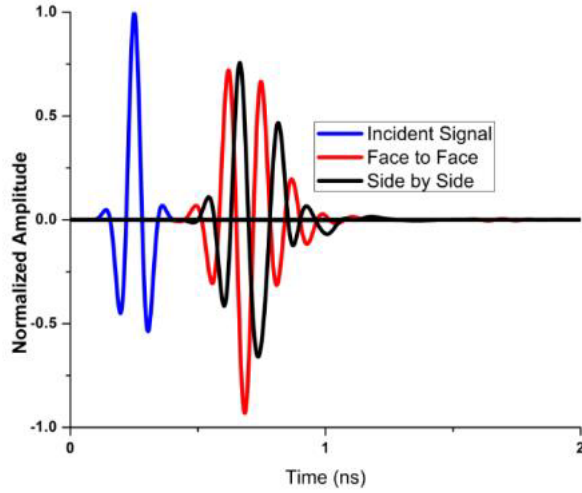
Figure 12. Normalized transmitted signal.
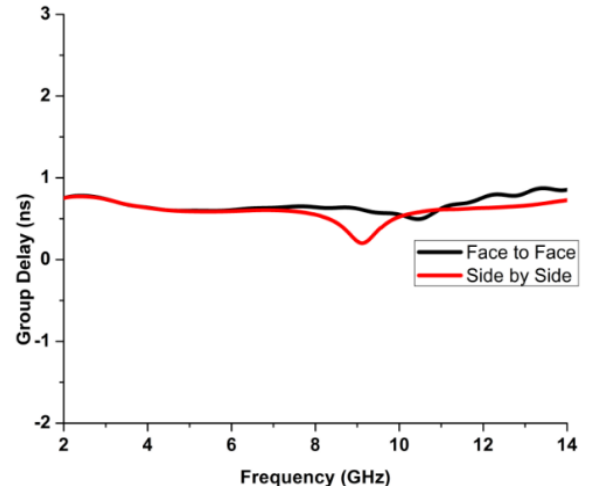
Figure 13. Group delay vs frequency and received signal.

(a)

(b)
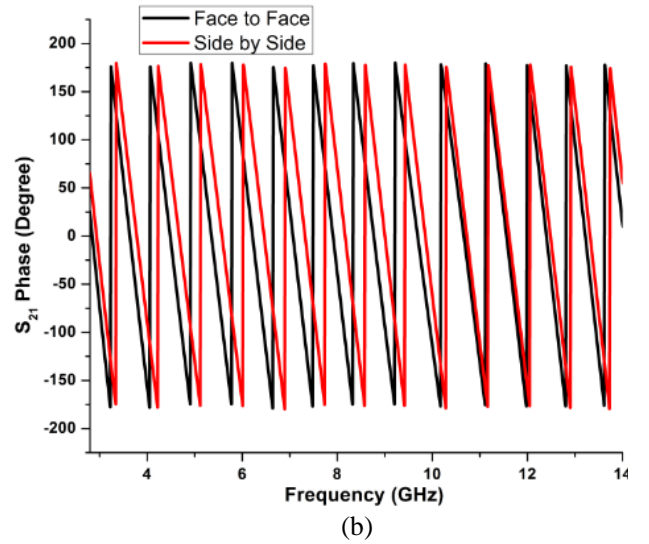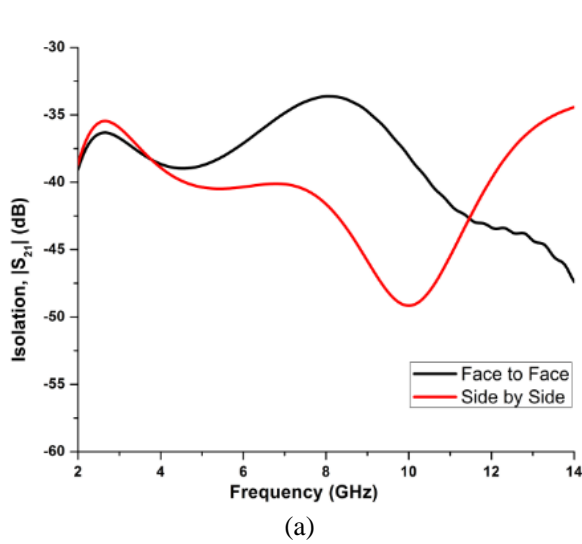
Figure 14. (a) Isolation (S_{21} (dB)) vs frequency and (b) phase of S_{21} vs frequency plot.

the isolation (S_{21}) magnitude is less than -33 dB, and the isolation phase has linear variations with frequency over the entire frequency band for both configurations, which implies that the system is highly correlated.

5. ON-BODY IMPLEMENTATION OF ANTENNA

A significant amount of electromagnetic energy is absorbed during the implementation of a wearable antenna on a human body. Therefore, it is necessary to determine biological effects on antenna performances and its EM radiation effects on the human body. Here, a cubic three-layered model is demonstrated as the human body, and Gustav voxel is used in the simulation software to determine biological effects. As seen in Figure 15, it comprises 3 layers of human body tissues: skin, fat, and muscle. The exhibited geometry has extents of 100 mm, 100 mm, and 46 mm in [25]. Material density and dielectric constant values used in the simulations at various frequencies are given in Table 2.

Figure 16 shows the setup for calculating biological effects on performances of the designed antenna
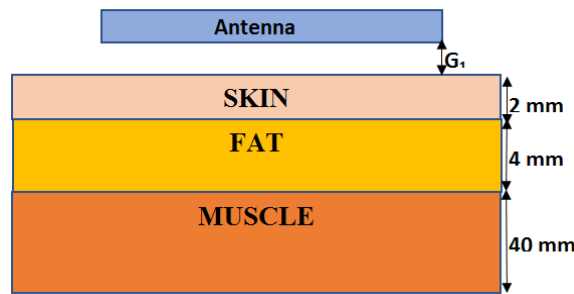
Figure 15. Cubic body tissue model used in the simulation.

| (a) | (b) | (c) | (d) |
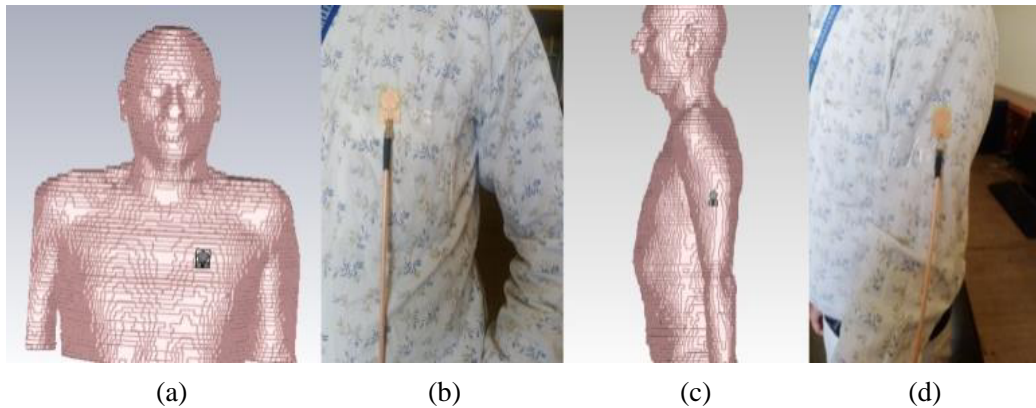
Figure 16. Set up for ON-body measurements when place antenna at (a) phantom chest, (b) real human chest, (c) phantom arm and (d) real human arm.

Table 2. Material properties of the human body tissues (frequency 1–20 GHz).

Tissue	Relative Permittivity	Density (kg/m^3)
Skin	40–25.75	1100
Fat	5.42–4.12	910
Muscle	54.3–32.1	1041

while the antenna is kept near a simulated model and real human body. Figure 17 depicts the antenna's simulated and measured S_{11} results in free-space and its implementation on different human body parts on a voxel model, real human chest, and arm. As depicted in Figure 17, the resonance frequency is shifted with slight impedance mismatching due to the homogenous dielectric medium of body tissues. However, these results validate that the designed antenna is still effectively operated in the entire UWB.

The impact on biological tissues is examined by SAR. The SAR is calculated by keeping the antenna on human phantom using following Equation (4)

$$S = \sigma E^2/\rho \tag{4}$$

where

S = Specified Absorption Rate (W/kg)

σ = Conductivity of human tissues (S/m)

E = Induced Electric Field in human tissues (V/m)

ρ = Density of human tissues (kg/m^2)
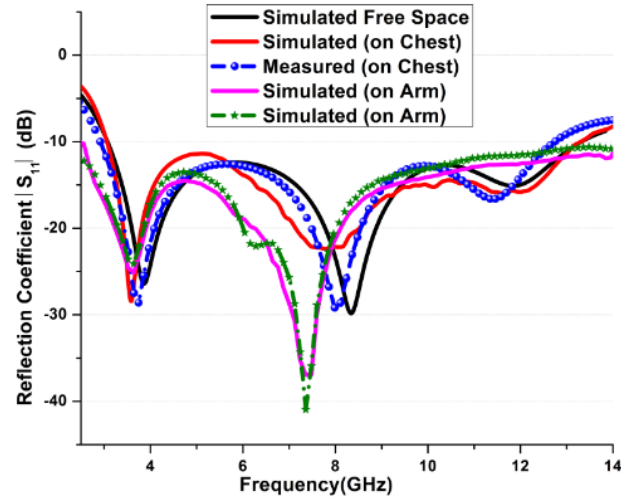
Figure 17. Simulated and measured S_{11} (dB) when placed at chest and arm.

(a)   (b)   (c)
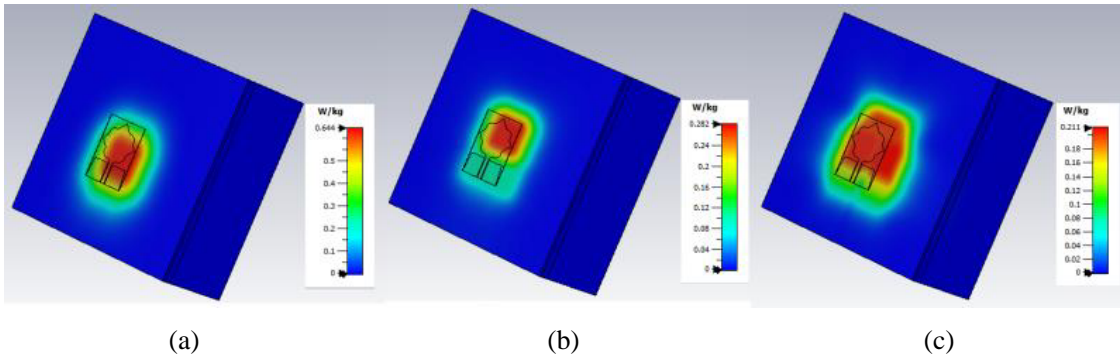
Figure 18. SAR analysis with three layer human phantom for 1 g tissues. (a) 3.7 GHz, (b) 8.4 GHz, (c) 11.2 GHz.

(a)   (b)   (c)
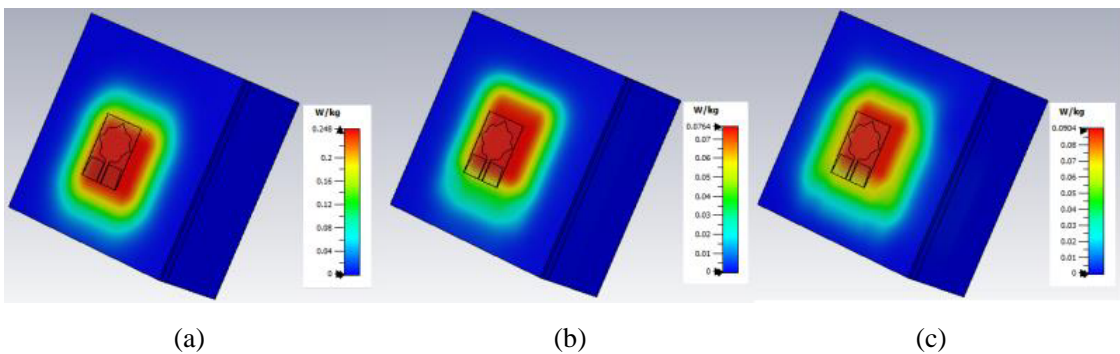
Figure 19. SAR analysis with three layer human phantom for 10 g tissues. (a) 3.7 GHz, (b) 8.4 GHz, (c) 11.2 GHz.

The SAR of the antenna was analysed with a three-layered flat phantom, on the chest and arm of the Gustav model at 3.7, 8.4, and 11.2 GHz frequencies. Figures 18(a) to (c) exhibit the SAR for 1 g tissue volume, and it is observed that given values less than the specified limit by the IEEEC9.5-1999 standard [25], these are 0.644, 0.282, and 0.211 W/kg at the frequencies as mentioned above. Similarly, Figures 19(a) to (c) display the SAR for 10 g tissues, i.e., 0.248, 0.0764, and 0.0904 W/kg at 3.7, 8.4 and 11.2 GHz frequencies.
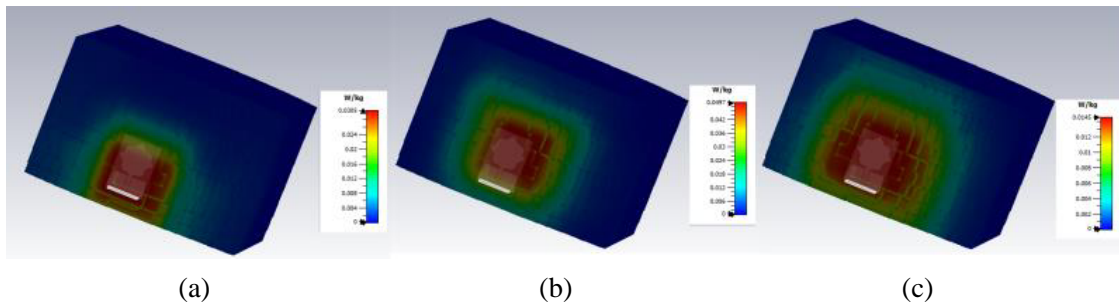
Figure 20. SAR when antenna placed at human phantom chest. (a) 3.7 GHz, (b) 8.4 GHz, (c) 11.2 GHz.

Furthermore, to investigate the effects on the human body, the antenna was kept near the chest and arm of the virtual human model, which was taken from the CST simulator. The SAR characteristics are investigated at 3.7 GHz, 8.4 GHz, and 11.2 GHz frequencies by placing this antenna on the human chest and arm at a 5 mm gap, and the corresponding results are plotted in Figure 20 and Figure 21. The obtained results show that the designed antenna satisfies the FCC, International Commission on Non-Ionizing Radiation Protection (ICNIRP) standards, indicating that the proposed antenna is safe for the human body. Table 3 presents a comparison between some recently reported UWB designs and the proposed antenna.

The above discussion shows that the proposed antenna has SAR under the limits recommended by the international standards. The omnidirectional radiation pattern of antenna makes it favourable

Table 3. Performance comparison between recently reported different antennas and proposed antennas.

Ref.	Size (mm^3)	Operating Band (GHz)	Material/ε_r	Flexible	Gain	SAR (W/kg)/Tissue/ Input Power (mw)
[6]	$40 \times 45 \times 0.5$	1.198 to 4.055	Polyester fabrics (2.193)	Yes	2.9 dBi	0.0014/10 g/1 at 15 mm distance from phantom
[7]	$30 \times 25 \times 0.8$	3.1–11.5	RT/Duroid (2.2)	Yes	5.25 dB	1.23 and 1.29/10 g/100 at 5 mm distance from arm and head
[11]	$30 \times 30 \times 0.7$	3.1 to 11.3	Felt (1.2)	Yes	4 dB	NR
[16]	$30.4 \times 38 \times 0.07$	3.06–13.5	Polyimide (3.5)	Yes	5.1 dB	NR
[17]	$50 \times 40 \times 0.8$ $50 \times 40 \times 0.728$	1.8 to 13.3	Polyamide (4.3) Teslin (2.23)	Yes	5.53 dBi 4.35 dBi	Min 1.41/1 g/100 at 10 mm distance from phantom
[19]	$50 \times 43 \times 0.2$ $50 \times 43 \times 0.8$	2.6 to 16	FR-4 (4.4) RT/Duroid	Yes	4.3 dBi	Min 1.268/10 g/100 at 10 mm distance from phantom
*	**$31 \times 22 \times 0.2$**	**3.08–13.6**	**FR-4 (4.4)**	**Yes**	**3.95 dBi**	**Min 0.0145/10 g/100 at 5 mm distance from chest**

*Proposed Antenna   NR: Not Reported

(a)   (b)   (c)
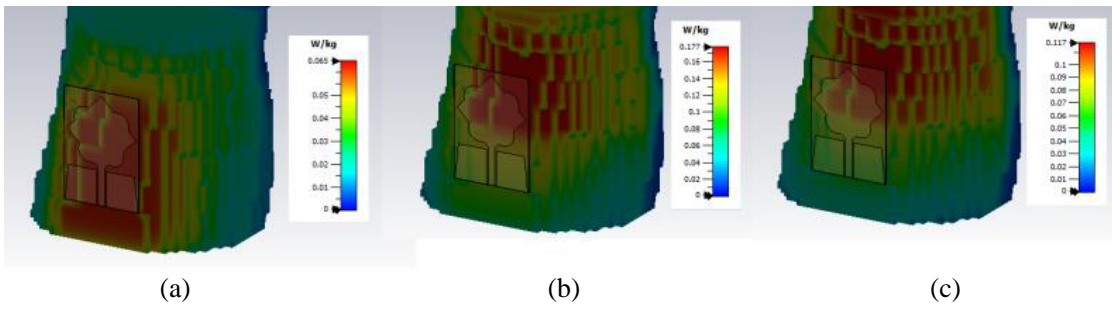
Figure 21. SAR when antenna placed at human phantom arm. (a) 3.7 GHz, (b) 8.4 GHz, (c) 11.2 GHz.

to communicate with other devices in BAN (Body Area Network) with controlled SAR; however, the added advantage of UWB antenna is that it consumes minimum power in the range of -41.3 dBm which controls the SAR within the limits. There are 3D radiation patterns summarized in Table 4 for the proposed antenna in various conditions like flat, bending along the X-axis, and bending along Y-axis.

Table 4. 3D radiation pattern plots of the proposed structure in different conditions.

S. No	Frequency (GHz)	Flat Condition	Bend along X-axis	Bend along Y-axis
1	3.7			
2	8.4			
3	11.2			

It is observed that the antenna maintains the omnidirectional characteristics at distinct frequencies; this can also be verified from the radiation patterns presented in Figure 8 and Figure 9.

The *FBR* (Front to Back Ratio) of the proposed antenna in various bending conditions is presented in Figure 22, and it can be observed that antenna has low FBR at lower frequencies, but it still produces satisfactory SAR, presented in Figure 18, Figure 19, Figure 20, and Figure 21, respectively. It is due to the low-level power consumption/radiation (range of milliwatts to microwatts) from the UWB antenna; however, at higher frequencies FBR is high which verifies that the proposed antenna has lower SAR than SAR values at lower frequencies.
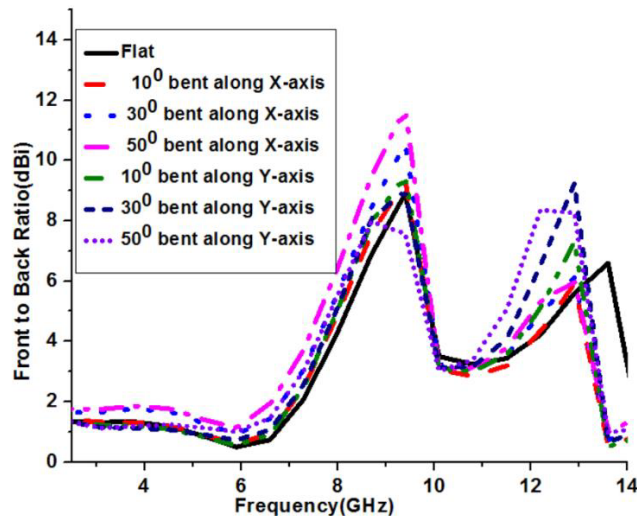
Figure 22. FBR performance of proposed antenna in X and Y axis bending conditions.

6. CONCLUSIONS

The radiation characteristic and biological impact on the human phantom of a CPW-fed monopole antenna for wearable applications are investigated. The demonstrated antenna was prototyped on a very thin substrate that is economical in comparison to other available substrates, and it has a very compact size as an added advantage for wearable applications. The physical robustness of the thin FR-4 substrate is tested by bending structure along the x and y-axes on cylindrical foam. This structure is suitable for ON body wearable applications and microwave imaging applications in various frequency bands like WLAN, WiMAX, LTE 42/43, and X-band. The impacts of antenna radiations on the human body were analysed through SAR calculation on the chest and arm, i.e., 0.0145 and 0.065 W/kg for 10 g tissue. The antenna has a peak realized gain of 4 dB, and its gains for bending states also have a very satisfactory range which makes it a desirable candidate for wearable applications. The validation of the proposed antenna has been done through frequency and time domain characteristics measurements.

REFERENCES

1. https://www.cdc.gov/coronavirus/2019ncov/hcp/telehealth.html for using Telehealth to Expand Access to Essential Health Services during the COVID-19 Pandemic(2019).

2. Yan, S., P. J. Soh, and G. A. Vandenbosch, "Wearable ultra wideband technology — A review of ultrawideband antennas, propagation channels, and applications in wireless body area networks," *IEEE Access*, Vol. 6, 42177–42185, 2018, https://doi.org/10.1109/ACCESS.2018.2861704.

3. Federal Communications Commission, First report and order, revision of Part 15 of Commission's rule regarding ultra-wideband transmission system FCC 02-48, Apr. 22, 2002.

4. Balani, W., M. Sarvagya, A. Samasgikar, T. Ali, and P. Kumar, "Design and analysis of super wideband antenna for microwave applications," *Sensors*, Vol. 21, No. 2, 477, 2021, https://doi.org/10.3390/s21020477.

5. Parameswari, S. and C. Chitra, "Compact textile UWB antenna with hexagonal for biomedical communication," *Journal of Ambient Intelligence and Humanized Computing*, 2021, https://doi.org/10.1007/s12652-021-03228-3.

6. Lin, X., Y. Chen, Z. Gong, B. Seet, L. Huang, and Y. Lu, "Ultrawideband textile antenna for wearable microwave medical imaging applications," *IEEE Transactions on Antennas and Propagation*, Vol. 68, No. 6, 4238–4249, 2020, https://doi.org/10.1109/TAP.2020.2970072.

7. Prudhvi Nadh, B., B. T. P. Madhav, M. Siva Kumar, M. Venkateswara Rao, and T. Anilkumar, "Circular ring structured ultra-wideband antenna for wearable applications," *International Journal of RF & Microwave Computer Aided Engineering*, Vol. 29, No. 4, e21580, 2019, https://doi.org/10.1002/mmce.21580.

8. Kumar, N. N., B. S. Srikanth, S. B. Gurung, S. Manu, G. N. S. Gowthami, T. Ali, and S. Pathan, "A slotted UWB monopole antenna with truncated ground plane for breast cancer detection," *AEU-Alexandria Engineering Journal*, Vol. 59, No. 5, 3767–3780, 2020, https://doi.org/10.1016/j.aej.2020.06.034.

9. Kumar, R., R. Sinha, A. Choubey, and S. K. Mahto, "An ultrawide band monopole antenna using hexagonal-square shaped fractal geometry," *Journal of Electromagnetic Waves and Applications*, Vol. 35, No. 5, 234–244, 2020, https://doi.org/10.1080/09205071.2020.1829094.

10. Hosseini Varkiani, S. M. and M. Afsahi, "Compact and ultra-wideband CPW-fed square slot antenna for wearable applications," *AEU-International Journal Electronics Communication*, Vol. 106, 108–115, 2019, https://doi.org/10.1016/J.AEUE.2019.04.024.

11. El Gharbi, M., M. Martinez-Estrada, R. Fernández-García, S. Ahyoud, and I. Gil, "A novel ultra-wide band wearable antenna under different bending conditions for electronic-textile applications," *The Journal of The Textile Institute*, Vol. 112, No. 3, 437–443, 2020, https://doi.org/10.1080/00405000.2020.1762326.

12. Zahran, S. R., M. A. Abdalla, and A. Gaafar, "New thin wide-band bracelet-like antenna with low SAR for on-arm WBAN applications," *IET Microwave Antennas Propagation*, Vol. 13, No. 8, 1219–1225, 2019, https://doi.org/10.1049/iet-map.2018.5801.

13. Hasan, Md. R., M. A. Riheen, Pr. Sekhar, and T. Karacolak, "Compact CPW-fed circular patch flexible antenna for super-wideband applications," *IET Microwave Antennas Propagation*, Vol. 14, No. 10, 1069–1073, 2020, https://doi.org/10.1049/iet-map.2020.0155.

14. Mustaqim, M., B. A. Khawaja, H. T. Chattha, K. Shafique, M. J. Zafar, and M. Jamil, "Ultra-wideband antenna for wearable internet of things devices and wireless body area network applications," *International Journal of Numerical Modelling: Electronic Networks, Devices and Fields*, Vol. 32, No. 6, 2590, 2019, https://doi.org/10.1002/jnm.2590.

15. Patre, S. R. and P. S. Singh, "CPW-fed flower-shaped patch antenna for broadband applications," *Microwave and Optical Technology Letters*, Vol. 57, No. 12, 2908–2913, 2015, https://doi.org/10.1002/mop.29480.

16. Zhang, Y., S. Li, Z. Q. Yang, X. Y. Qu, and W. H. Zong, "A coplanar waveguide-fed flexible antenna for ultra-wideband applications," *International Journal of RF & Microwave Computer Aided Engineering*, Vol. 30, No. 8, 1–11, 2020, https://doi.org/10.1002/mmce.22258.

17. Reddy, B. N. B., P. S. Kumar, T. R. Rao, N. Tiwari, and M. Balachary, "Design and analysis of wideband monopole antennas for flexible/wearable wireless device applications," *Progress In Electromagnetics Research M*, Vol. 62, 167–174, 2017, https://doi.org/10.2528/PIERM17092107.

18. Elmobarak Elobaid, H. A., S. K. Abdul Rahim, M. Himdi, X. Castel, and M. Abedian Kasgari, "A transparent and flexible polymer-fabric tissue UWB antenna for future wireless networks," *IEEE Antennas and Wireless Propagation Letters*, Vol. 16, 1333–1336, 2017, https://doi.org/10.1109/LAWP.2016.2633790.

19. Negi, D., R. Khanna, and J. Kaur, "Design and performance analysis of a conformal CPW fed wideband antenna with Mu-negative metamaterial for wearable applications," *International Journal of Microwave and Wireless Technologies*, Vol. 11, No. 8, 806–820, 2019, https://doi.org/10.1017/S1759078719000497.

20. Yadav, A., V. Kumar Singh, A. Kumar Bhoi, G. Marques, B. Garcia-Zapirain, and I. de la Torre Díez, "Wireless body area networks: UWB wearable textile antenna for telemedicine and mobile health systems," *Micromachines*, Vol. 11, No. 6, 558, 2020, https://doi.org/10.3390/mi11060558.

21. Martínez-Lozano, A., C. Blanco-Angulo, et al., "UWB-printed rectangular-based monopole antenna for biological tissue analysis," *Electronics*, Vol. 10, 304, 2021, https://doi.org/10.3390/electronics10030304.

22. Varshini, K. and T. R. Rao, "Thermal distribution based investigations on electromagnetic interactions with the human body for wearable wireless devices," *Progress In Electromagnetics Research M*, Vol. 50, 141–150, 2016, https://doi.org/10.2528/PIERM16071703.

23. Gupta, N. P., M. Kumar, and R. Maheshwari, "Development and performance analysis of conformal UWB wearable antenna under various bending radii," *IOP Conference Series: Materials Science and Engineering*, Vol. 594, 012025, 2019, http://dx.doi.org/10.1088/1757-899X/594/1/012025.

24. Song, L. and Y. Rahmat-Samii, "A systematic investigation of rectangular patch antenna bending effects for wearable applications," *IEEE Transactions on Antennas and Propagation*, Vol. 66, No. 5, 2219–2228, 2018, https://doi.org/10.1109/TAP.2018.2809469.

25. Sharma, M. D., A. Yadav, S. Singhal, and R. Sharma, "Design and simulation of flower shaped flexible wideband antenna for WBAN applications," *IEEE Indian Conference on Antennas and Propagation (InCAP)*, 140–143, 2021, https://doi.org/10.1109/InCAP52216.2021.9726448.